Corrosion Science 131 (2018) 147–155

Contents lists available at ScienceDirect

Corrosion Science

journal homepage: www.elsevier.com/locate/corsci

The effect of work-hardening and thermal annealing on the early stages of the uranium-hydrogen corrosion reaction

A. Banos*, C.P. Jones, T.B. Scott

University of Bristol, Interface Analysis Centre, School of Physics, HH Wills Physics Laboratory, Tyndall Avenue, Bristol, BS8 1TL, United Kingdom

ARTICLE INFO

Keywords:
B. SEM
SIMS
C. effects of strain
Hydrogen permeation
Interfaces
Pitting corrosion

ABSTRACT

The characteristics of hydride formation on metallic U at the early stages were investigated for three differently treated samples. The first sample reacted in its as-received state, the second was thermally annealed and the third sample underwent cold work-hardening prior to reaction with deuterium. From the analysis, the vacuum heat-treated sample was found to be more resilient to hydriding at the nucleation and growth stage, exhibiting a reduced number of nucleation points when compared to the as-cast uranium. The work-hardened sample was observed to be more susceptible to H_2 corrosion, displaying very dissimilar hydriding behaviour when compared to the other.

1. Introduction

Hydrogen corrosion of metallic U may occur during various stages of the nuclear fuel cycle, however, it is predominantly observed to occur during waste disposal [1–3]. The formed corrosion product, uranium hydride (UH_3), is a highly pyrophoric and unstable substance and, therefore, classed as a potential hazard due to the potential for enhanced radionuclide release and dispersion of gas/solid fission products arising from the spent nuclear fuel (SNF) material (fire, smoke containing fission products, etc.) [4,5]. The reaction can be described by four distinct stages:

i. The induction period (Initial hydrogen adsorption).
ii. The nucleation and growth period (Discrete UH_3 sites form and grow).
iii. The bulk reaction period (Adjoining UH_3 sites create a reaction front that engulfs the surface and progresses inwards consuming the U metal).
iv. The termination period (Complete transformation of U to UH_3).

Prior to the bulk reaction stage, the rate of which is mainly governed by the conditions of the surrounding environment [6–15], the nucleation and growth stage occurs in a spot-wise manner where hydrides begin to form and grow at certain regions of the metal surface [16]. These regions are assumed to act as low energy points where hydrogen molecules can quickly and easily physi-sorb, chemisorb, dissociate and reach the metal surface to react [16]. The nucleation and growth period is rapid and far more complex than any other stage of the uranium-hydrogen system. There are a number of factors controlling the nucleation rate and density of the UH_3 formation, along with the topography and morphological characteristics of the hydrides [16–26]. Increasing oxide thickness has a diminishing effect on the hydride nucleation rate and density [21]. However, this results in larger and more developed hydrides [21]. An impure reactant gas (H_2, D_2, etc.) would eventually cause the nucleation number density to shrink, owing to the competition between hydrogen and other diffusing entities (CO, O_2, N_2, H_2O) on the existing sorption sites [18]. Saturation of the available sorption sites for hydrogen may appear if the level of surface and/or oxide impurities prior to the reaction is significant [21]. The pressure and temperature of the reaction determine the flux of hydrogen (H_2) from the gas phase to the metal [27]. Thus, the rate of nucleation will increase exponentially with temperature up to the maximum value where hydriding is conceivable ($\sim$260 °C), provided that H_2 pressure is adequate [27]. However, the nucleation number density is finite for certain conditions, since the solubility of hydrogen in uranium is solely controlled by temperature and metal microstructure [17]. Temperature may also affect the location of hydriding initiation and growth to a certain extent [22,28,29]. Working on early stage hydriding of a well-annealed depleted uranium sample at the high-temperature regime ($\geq$240 °C), Scott et al. [22] found that hydrides nucleated mainly across high misorientation angle grain and twin boundaries, forming chains instead of distinct spots [22].

The surface characteristics, including the metal microstructure, play the most dominant role with respect to the location of hydriding initiation and the overall hydriding behaviour at the early reaction stage [20,22]. Strain on the surface manifested as scratching lines, or a work-

* Corresponding author.
E-mail addresses: antonisbanos@gmail.com, antonis.banos@bristol.ac.uk (A. Banos).

https://doi.org/10.1016/j.corsci.2017.11.017
Received 29 September 2016; Received in revised form 10 November 2017; Accepted 11 November 2017
Available online 14 November 2017

hardened layer, is either a result of mechanical abrasion during experimental preparation or as a result of stripping off coating material, such as Magnox from a spent nuclear fuel rod, in a real-world scenario. Surface strain typically affects the hydriding behaviour and morphology of the hydrides [30,31]. Very recent work by Banos et al. [30], working on natural uranium samples prepared using mechanical abrasion, revealed that it is the level of surface strain that controls hydriding parameters such as nucleation rate, density and location of the hydrides. Additionally, for chemically etched and strain-free surfaces, the microstructure was deduced to control the population and location of surface-formed hydrides [30]. Complementary work on natural uranium, by employing electron back-scattered diffraction (EBSD) to map a partially hydrided uranium surface, was undertaken to evaluate and quantify the effect of the various characteristics of metal microstructure on UH_3 site initiation [32]. From analysis of the electropolished and partially hydrided surface, it was established that more than 90% of the observed UH_3 sites formed around grain and twin boundaries [32]. From both these works, it was concluded that when a work-hardened layer is present on the surface, discontinuities in the microstructure which are also reflected as discontinuities in the superficial oxide, act as preferential sites for UH_3 nucleation and growth [30,32]. However, for a more pristine surface, it is the metal microstructure and grain/twin boundaries, which exert a greater control on the abundance and location of the forming hydrides [30,32]. Therefore, if the grain boundary length is diminished (grain growth) and the level of internal stresses are reduced (annealing), it is expected that a pristine surface will exhibit fewer preferential points for successful initial hydrogen attack. Likewise, on a surface with a well-developed work-hardened layer, surface strain and an increased grain boundary length, developed through slip twinning, is expected to strongly influence early hydriding behaviour.

This work was focused on comparing and evaluating the early hydriding characteristics of three samples that have undergone various treatments prior to reaction, to create comparable differences in surface strain. To achieve this, the first uranium sample was reacted in its as-received state (as-cast), while the second sample was thermally annealed to relieve strain imbued during fabrication, whilst also encouraging grain growth. The third sample was deliberately cold-work polished to induce a superficial work-hardened layer of significant thickness. All three samples were loaded into the same cell and reacted together to ensure identical reaction conditions.

2. Experimental

2.1. Sample characterisation

Unirradiated natural uranium metal, prepared as fuel rod material for Magnox reactors, and used in previous works [30,32], was used for the study. Table 1 displays the composition of the metal, as determined by energy dispersive X-ray (EDX) analysis. The main impurities in the metal were C, N, O, Al, Si and Fe. C, N and O impurities were considered as over-estimated owing to (a) carbon deposition from residual hydrocarbon disintegration by the action of the electron beam and (b) the ubiquitous presence of a surface oxide film, and (c) amplification of the signal coming from the low mass elements (over the heavy elements), for low accelerating voltages [33–35]. Preliminary scanning electron microscopy (SEM) inspection of the surface revealed carbides and carbo-nitrides of varied morphology. The samples exhibited a high carbon content with approximately 820 ± 270 carbides/mm^2 on the polished surface; the mean diameter of the carbides was estimated to be 7 ± 4 μm (Fig. 1a). The carbide number density was found to change across the samples, with regions close to the edge of the original fuel bar exhibiting a higher number density than regions corresponding to the centre-line. This variation is generally well accepted to occur as an unavoidable part of the fabrication process.

Table 1
Level of impurities detected through energy dispersive X-ray (EDX) analysis of Magnox-U. 1.

Element	*Impurity level in (wt%)*
U	88.15 ± 1.32
C	12.37 ± 0.81
N	1.94 ± 0.20
O	1.73 ± 0.87
Al	0.20 ± 0.06
Si	0.06 ± 0.04
Fe	0.00 ± 0.37

Metal grains with linear variation in size and random orientation were developed during the initial casting and subsequent β-quenching of the material. This fabrication process also resulted in internal stress development which was manifested as multiple slip planes and twin boundaries between the grains (Fig. 1b). Three square samples of the same weight, shape and surface area (~0.45 g, 4.6 × 4.6 × 2 mm) were cut from the virgin Magnox-U metal by employing a Struers accutom cutting machine. This process was expected to cause some surface mechanical disruption to the cut surfaces of the samples.

2.2. Sample treatment

Following mechanical sectioning, three distinct treatment methods were employed to induce different levels of internal and external strain on the surface.

Sample 1: As-cast uranium. The first sample was used in its as received state (as-cast uranium).

Sample 2: Thermally annealed uranium. The second sample was loaded into a stainless steel cell with silver-coated copper gasket seal and heat-treated under high vacuum (5×10^{-7} mbar or 5×10^{-5} Pa) at 550 °C for 140 h. Following annealing, the cell was left to cool to ambient temperature under vacuum over a 20 h period. The annealing encouraged grain growth and recrystallisation, which has been found to initiate at temperatures as low as 450 °C [19]. This heat treatment also led to relief of residual mechanical strain present as a result of the manufacturing process [19].

Sample 3: Work-hardened uranium. The final sample underwent cold work-hardening using Buehler silicon carbide grit papers to produce a coarse finish (P320, 46 μm) followed by finer finish (P600–P1200) to produce a work-hardened layer of significant thickness (3–6 μm, Fig. 2b). Fig. 2a & b present focused ion beam (FIB) cross-sectional views of the as-cast uranium and the work-hardened sample. It is evident that the thickness of the disrupted layer owing to mechanical damage is increasing while the level of strain along this layer is multiplied.

Fig. 3a–c show the EBSD maps of each sample surface. To produce a surface pristine enough for EBSD mapping, the samples were mechanically polished down to a ¼-μm surface finish and electrochemically etched, using a solution containing a 10:6:6 (volume ratio) mixture of ethylene glycol, orthophosphoric acid and absolute ethanol, with an applied voltage of 10–11 V and a flowing current of ~0.1 A for less than 1 min. Consequently, the samples were loaded separately into the FIB and the surface was sputtered using a beam current of 2700 pA for ~10 min at an incident angle of 7° to the surface, in order to reveal the metal microstructure. On the as-received sample (Fig. 3a), multiple grains and twin boundaries of various sizes were clearly identified. Fig. 3b presents the EBSD map of the thermally annealed sample. It is evident that some grain growth has occurred on the surface, along with considerable strain relief, manifested as a reduction in the density of crystal twins present. The work-hardened surface exhibited a greater number density of twin boundaries when compared to the other two surfaces, along with significant damage leading to splitting of the large grains to smaller sub-grains (Fig. 3c). Fig. 4 demonstrates the spread of the grain size (in area fraction) for all three mapped surfaces. From the figure, it can be seen the as-cast uranium surface exhibits grains of

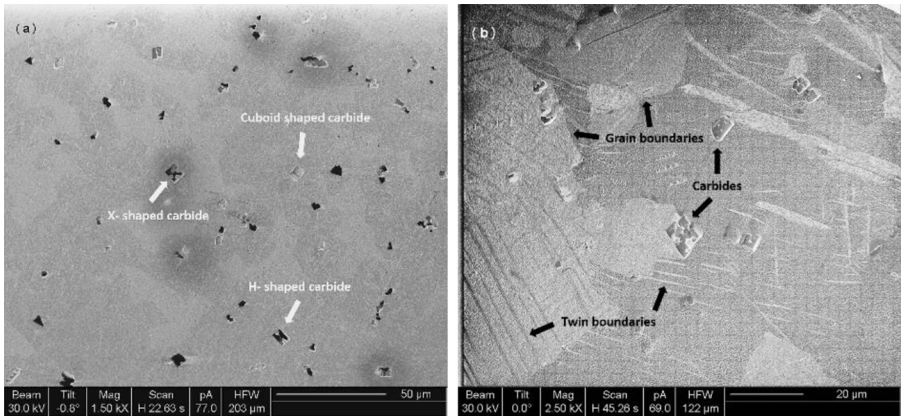

Fig. 1. Secondary electron (SE) images showing the surface of a Magnox-U sample with high carbon content. The sample was a) nitric-acid etched and b) electropolished, followed by ion-sputter cleaning using a focused ion beam (FIB) milling instrument (2700 pA, 10 min, 0.04 mm2, angle of incidence: 7°) to reveal the microstructural features of the surface.

various sizes, with less than 26% of the mapped area covered with grains larger than 54 µm while on the thermally annealed sample around 55% of the mapped surface is covered with large grains (~71 µm). Enhanced grain size confirms the relaxation effect of thermal heat treatment. On the work-hardened sample, the grain size was limited to a maximum value of ~15 µm on the mapped surface. This effect was a result of disruption and distortion of the surface, leading to splitting of the larger grains of the sample to smaller sub-grains. However, it is worth noting here that, for more quantitative data, mapping of larger areas is required, with the average area fractions statistically computed and compared.

2.3. Surface preparation

Except for the work-hardened surface which was mechanically abraded from P1200 paper grit directly to the highest surface finish used (P4000), all remaining samples were subsequently mechanically abraded with successively finer grades of SiC grit paper to remove the work-hardened damage of the previous grade up to P4000 level (2 − 3 µm surface finish). The samples were washed together in ethanol and ultra-high purity methanol, to ensure that any residual surface impurities were removed, and left exposed to air for 10 min to dry before being weighed. All samples, at the point of subsequent hydrogen exposure, had comparable surface oxide thicknesses.

2.4. Hydriding reaction

Following surface preparation, all three samples were loaded together in a stainless steel reaction cell and evacuated to $< 5 \times 10^{-7}$ mbar (5×10^{-5} Pa). Thin aluminium foil sheets were used to hold the samples apart in the cell ensuring no contact, interaction or material exchange between the samples took place, whilst allowing hydrogen easy access to the surface. Additionally, at the temperatures and pressures of gas used, the proximity of each sample to the gas inlet was not expected to affect the sample hydriding rate due to the high mobility of hydrogen within the cell. The temperature was initially raised to 120 °C and the samples were degassed for ~2 h. This period was considered sufficient for the majority of oxide impurities to desorb but without significant oxide diffusion/transformation [23,25] or metal grain growth [19,36] occurring. A second increase to the reaction temperature was followed (190 °C − left to stabilise for 1 h) and a fixed volume of deuterium (D_2) was introduced into the system at 500 mbar (50 kPa). Isotopic labelling of the reacting gas was chosen for two reasons: 1) deuteride growths were more easily traced on the mapped regions when secondary ion mass spectrometry (SIMS) was employed; and 2) deuterium is chemically identical to hydrogen as a reactive agent for uranium. Thus, in the following text, terms such as hydride/hydriding may be considered equivalent to deuteride/deuteriding.

Upon deuterium admittance to the reaction cell, an almost immediate and continuous drop in gas pressure was observed signifying the onset of hydride nucleation and growth. The reaction was ceased after a measured drop in deuterium pressure of 1.4 mbar (140 Pa) was recorded, equivalent to 0.00263 mmol of D_2 consumed to form UD_3. That quantity was considered appropriate to initiate hydride formation and growth without reaching the bulk stage of the reaction.

2.5. Analysis techniques

2.5.1. Secondary ion mass spectrometry (SIMS)

The secondary ion mass spectrometry work was carried out using a custom-made SIMS instrument as in [32]. A FEI focused gallium ion source combined with a Vacuum Generators model 7035 double focusing magnetic sector mass analyser comprised the set-up. The analysis was performed in positive ion mode with a 3 nA beam current.

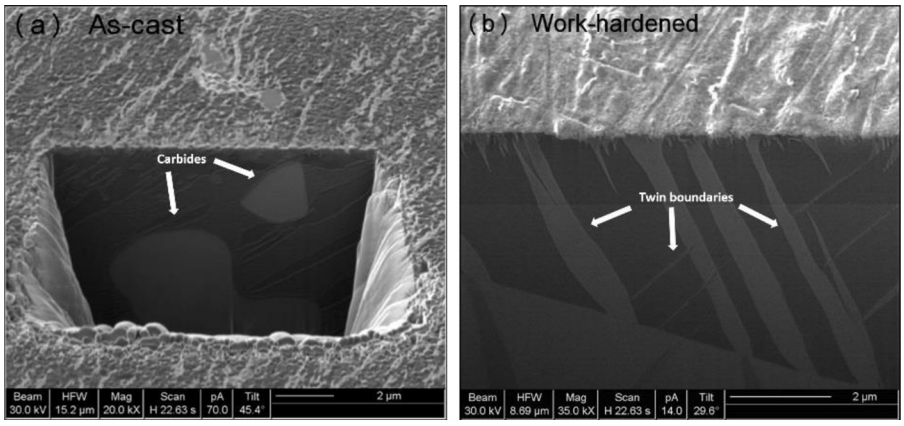

Fig. 2. Secondary electron (SE) images showing focused ion beam (FIB) milled cross-sectional views of (a) as-cast uranium and (b) work-hardened uranium. Stress-induced twins from work-hardening are clearly seen to extend several micrometres into the bulk uranium.

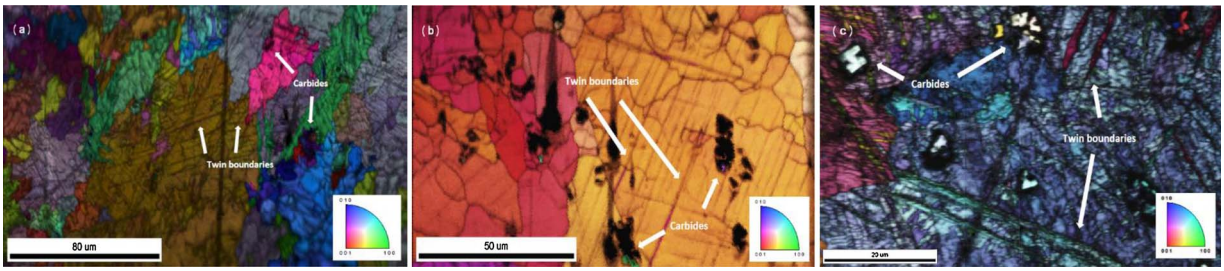

Fig. 3. Electron back-scattered diffraction (EBSD) maps of (a) as-received uranium (as-cast) (b) thermally annealed uranium (550 °C, 140 h) and (c) work-hardened uranium. From the maps it is clear that (i) the twin boundaries are lessened on (b)-(thermally annealed surface) when compared to (a)-(as-cast uranium) and (ii) the work-hardened surface (c) exhibits the most disrupted surface with multiple twin boundaries along with general observed distortion.

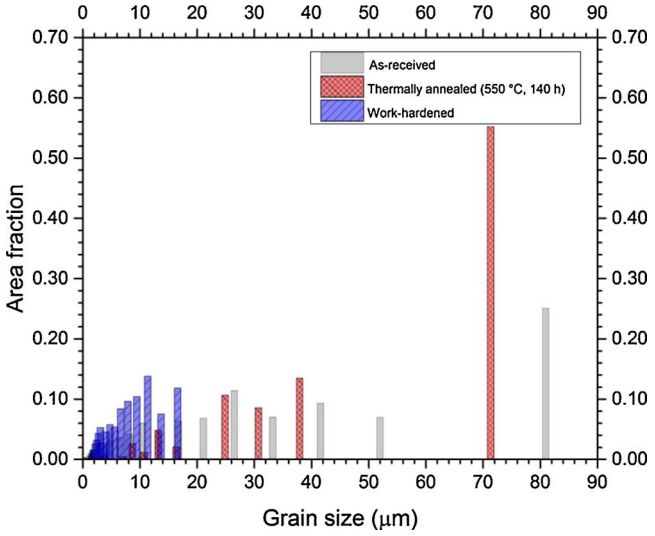

Fig. 4. Spread of the grain size covering the uranium surface for a finite mapped region of the as-cast (grey), thermally annealed (light red) and work-hardened (light blue) samples (in area fraction). The as-cast uranium exhibits linear variation in grain size when compared to the other two surfaces. Thermal annealing results in an increase in the grain size while on the work-hardened sample, damage on the surface breaks the larger grains into smaller ones. (For interpretation of the references to colour in this figure legend, the reader is referred to the web version of this article.)

UD^+ mass ion maps in various regions and for all three surfaces were obtained to identify the hydride sites. Fig. 5a–d provide examples of how hydride sites have been detected on the as-cast and work-hardened uranium surfaces. Combining SIMS mass ion maps with SEM and FIB images allowed us to identify the UH_3 sites through a very large number of regions representative of the sample surface. The derived number density from every image/map was extrapolated for mm^2 and the mean value from all these numbers provided the nucleation number density for each sample.

2.5.2. FIB milling and rastering – secondary electron (SE) imaging

The same FEI FIB-201 instrument as in [30,32] and a Helios Nanolab 600i dual beam system were used for preliminary and post-hydriding interrogation of each surface. Microstructural features of the surface were revealed by ion-raster scanning at an angle of incidence between 5 and 10° (2700–6600 pA, 30 kV). Cross-sectional cuts were made on all surfaces in an effort to gain information on the post-treatment state of the samples prior to the reaction and identify the hydride nucleation locations at the post-hydriding stage. SE imaging was conducted using a low beam current (70 pA) with an accelerating voltage of 30 kV.

2.5.3. EBSD analysis

Preliminary analysis and characterisation of the surface were conducted using a Zeiss EVO-MA10 SEM instrument with LaB_6 source operating with an accelerating voltage of 30 kV and a probe current of 0.7 nA. EBSD patterns were obtained by acquiring the signals from a phosphor control screen with a Digiview 3 high-speed camera while data collection and processing were conducted by a supporting EDAX-EBSD instrumentation fitted with orientation imaging microscopy Analysis 6.2 software as in [30,32].

3. Results

Fig. 6 illustrates the physical appearance of all three surfaces after the hydriding reaction. From direct observation, it is evident that the first two samples (as-cast, thermally annealed) exhibit similar hydride and surface characteristics, contrasting with the work-hardened sample. The type of attack on the work-hardened surface was notably different with the hydrides forming around discontinuous areas and following fractured regions of the oxide, ascribed to the prior mechanical processing. The most notable hydriding characteristics for the three samples are displayed on Table 2. The number density of hydrides on the work-hardened sample was lower than the as-cast and thermally annealed samples but the size of the hydrides and the extent of hydriding damage across the surface was considerably higher, with many of the observed hydrides having breached the confining oxide layer, unlike the other samples. As expected, carbide inclusion margins were found to act as preferred sites for nucleation of UH_3 growth (Fig. 7a–c). From the analysis, it was established that more than half of the inclusions on all three surfaces accommodated hydrides on their periphery (Table 2).

3.1. As-cast uranium sample

The as-cast uranium exhibited the highest hydride growth density, 2300 ± 700 hydrides/mm^2 (Table 2). The hydrides displayed lenticular/crescent-like shape across the surface. The mean diameter of the spots was measured at ~4.3 ± 1.5 μm (Table 2), with an average maximum cross-sectional depth of 0.7 ± 0.3 μm. Hydride development was not observed to breach the superficial oxide layer. Grain/twin boundaries (Fig. 8a) and carbide inclusions (Fig. 8b) were observed to act as preferred sites for nucleation of hydride growths. The carbide number density was also found to vary across the sample surface, commensurate with the variation in hydride number density. This was attributed to a variation in carbon content from the centre-line to the edge of the precursor fuel rod.

3.2. Thermally annealed uranium sample

The thermally annealed sample exhibited the least residual stress and surface damage. The hydride nucleation number density on this sample was slightly lower than on the as-cast uranium, at 1950 ± 630 hydrides/mm^2 (Table 2). The diminished number density of hydride sites was ascribed to an assumed reduction in the number of twin and grain boundaries owing to grain growth with concurrent stress relief. The mean diameter of the hydride spots was ~3.8 ± 1 μm with no

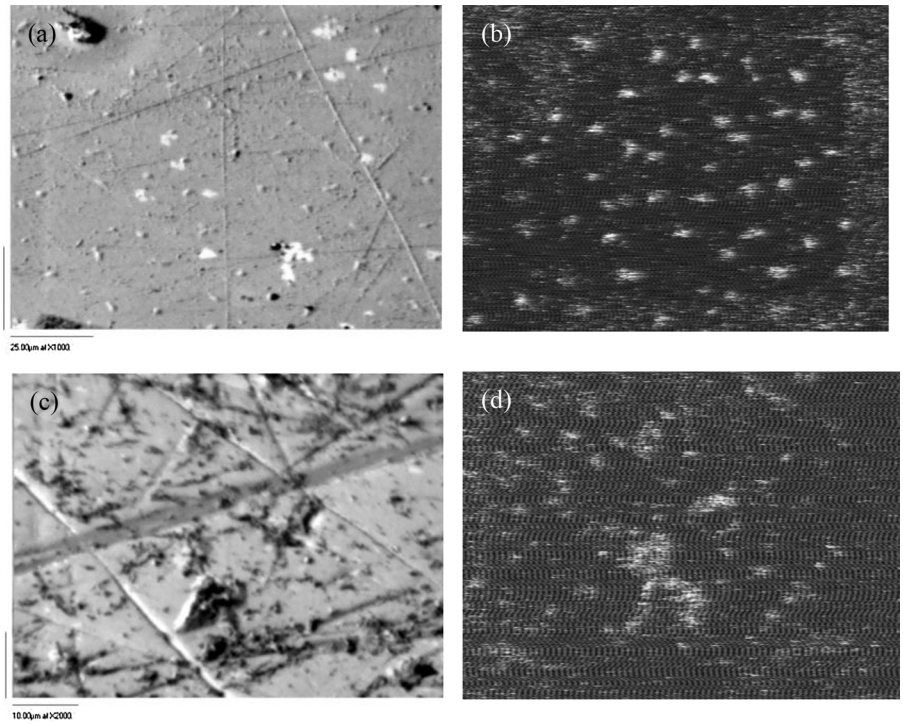

Fig. 5. Secondary electron (SE) images of the partially hydrided surface of (a) as-cast and (c) work-hardened sample with (b) and (d) (same scale as (a) and (c)) corresponding mass ion maps for the UD+ ion cluster. It is clear that regions of enhanced ion yield (brighter areas in (b) and (d)) are coincident with observed blister-like or disrupted regions on (a) and (c), establishing that these regions are uranium hydride growth locations.

sites seen breaching the oxide layer and an average maximum cross-sectional depth of 0.7 ± 0.3 μm. Fig. 9a & b display the thermally annealed and partially hydrided surface prior to and following ion-sputtering. From close observation of the sputtered surface (Fig. 9b), it is evident that hydride growth and development occurs close to or at grain and twin boundaries. Additionally, almost two-thirds of the observed carbides acted as nucleation sites for hydride growth (Fig. 10 & Table 2).

3.3. Work-hardened uranium sample

The work-hardened sample displayed the lowest number density of hydride growths (550 ± 500 hydrides/mm^2). In the work-hardened surface two families of hydrides were observed to have formed: (1) a small diameter nucleating group associated mostly with grain/twin boundaries and surface strained regions; and (2) a group of large oxide-ruptured nucleation sites, observed to form around carbides, oxide discontinuities and fractured regions (Fig. 11a & b). This behaviour has been observed previously by Jones et al. [37] and, in this work, was unique to this particular method of sample surface preparation. This latter group, accounting proportionally ~10% of the nucleation sites, consisted of hydrides 16.2 ± 6 μm in maximum dimension, with the majority having breached the surface oxide layer. Significant vertical hydride growth (into the sample) was only evident on this sample, with hydride propagation to a mean depth of 3 ± 0.5 μm.

4. Discussion

In this work, we have attempted to test how hydride formation behaviour is altered by deliberate alteration of the microstructure and strain levels of the metal surface. From previous work, it was established that grain and twin boundaries exert a control on hydride growth location by providing preferred sites for nucleation [32]. In the present work, we reduced the overall grain and twin boundary length by subjecting one of the samples to thermal annealing for prolonged periods. The thermal treatment encouraged recrystallisation, grain growth and the release of residual internal stress present within the bulk uranium. This was clearly evidenced in the EBSD data (Figs. 3 and 4). One additional effect of the thermal treatment on the sample could potentially be the liberation of hydrogen trapped during the casting process and accommodated within the bulk of the metal [38]. When uranium metal is held at elevated temperatures for prolonged periods under vacuum, a proportion of any entrapped hydrogen will diffuse out from the bulk metal [39]. Hence, the annealing treatment will have reduced the

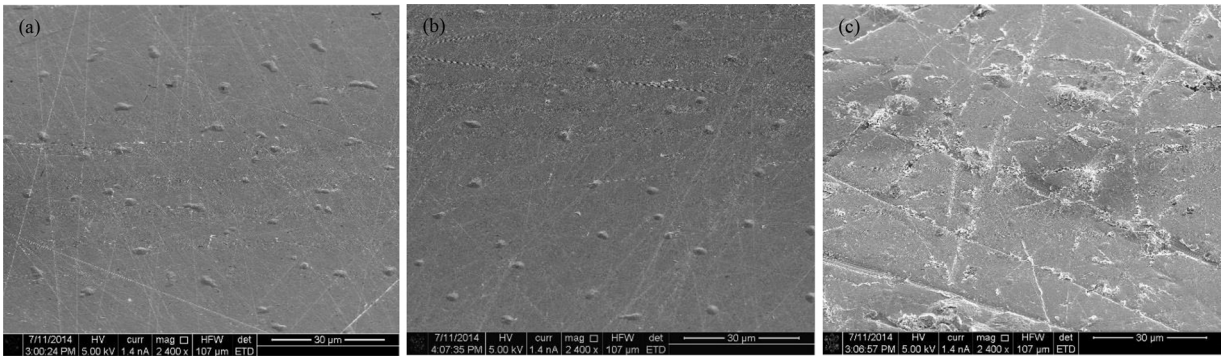

Fig. 6. Secondary electron (SE) images of Magnox-U hydrided samples showing (a) the as-cast; (b) the thermally annealed and (c) the work-hardened surfaces after partial reaction under 500 mbar (50 kPa) D2 at 190 °C.

Table 2
The hydriding parameters of all three reacted surfaces.

Sample	*Spatial density (hydrides/mm^2)*	*Small hydride diameter (μm)*	*Large hydride diameter (μm)*	*Percent of hydrides associated with grain/twin boundaries (%)*	*Percent of carbides accommodating hydride(s) on their peripheries (%)*
As-cast	2300 ± 700	4.3 ± 1.5	n/a	~73	~57
Thermally-annealed	1950 ± 600	3.8 ± 1	n/a	~71	~63
Work-hardened	550 ± 500	4 ± 2	16.2 ± 6	~74	~53

amount of microstructure-entrapped hydride that was inherited through the fabrication process.

Opposite to reducing surface strain using annealing, we also increased surface strain and grain boundary length in one sample using mechanical work hardening. The level of damage on this sample was significant and, thus, we would argue, closer to a real-case scenario where the surface of the uranium rods is may be physically strained due to (1) mechanical disruption from fuel cladding removal and (2) strain induced by in-reactor irradiation damage.

The thermally annealed sample exhibited slightly lower hydride nucleation number density when compared to the as-cast uranium sample (Table 2). This was expected since the grain and twin boundary length per unit area and internal residual stresses were deliberately reduced. A slight increase in the apparent influence of carbide inclusions as desirable sites for UH_3 nucleation was also observed on the thermally annealed sample (Table 2). Since the carbides are not considerably affected by the thermal treatment, the carbide margin to grain-twin boundary length ratio increases and, thus, carbide locations become of greater importance as preferential H_2 attack points on the thermally annealed sample.

For metal samples with lower carbon content i.e. lower carbide number density, a more pronounced difference in hydride nucleation number density between as-cast and thermally annealed sample would be expected. A very recent work from Petherbridge et al. [40] investigated the effect of thermal treatments and cycles (35–75 °C) on the nucleation and growth of UH_3 on uranium. They found that the nucleation kinetics were enhanced (shorter induction period, higher number of UH_3 sites per unit area over the same time period) on metal which had undergone a precursor thermal cycle in comparison metal which had not. They hypothesised two potential processes leading to this behaviour: (i) disruption of the superficial oxide layer arising from temporal distortion of the underlying parent uranium due to its differential (anisotropic) thermal expansion, and (ii) differences in the cleanliness of the surface oxide layer in relation to absorbed or entrapped contaminant species (OH^-, H_2O, CO_2, etc.). Their findings may appear contradictory to this work, however, there are several significant differences between the studies. Firstly, the thermal annealing cycle applied in this work was at a considerably higher temperature (550 °C versus 35 − 75 °C for Petherbridge) and for a significantly greater period (140 h versus 16 h) allowing the sample to recrystallise and reduce its internal strain. Such, recrystallization and stress relief cannot be observed in samples which are thermally cycled below 450 °C and for short periods [19]. Secondly, subsequent to the annealing process the treated sample was subjected to the same surface preparation as the other samples, with all samples being degassed together in the same cell prior to reaction. It is thus expected that after the degassing period (120 °C, 2 h – 190 °C, 1 h) similar levels of oxide contamination from absorbed and entrapped species would have existed on all three samples. Hence, diffusion kinetics through the oxide and nucleation will be similar for all three samples. In this case, under identical H_2 corrosion conditions, only the microstructure and surface strain will affect the nucleation process.

For Petherbridge's hypothesis (i), which argues promotion of hydride formation due to oxide disruption caused by anisotropic thermal expansion of the underlying metal, our thermally annealed sample would be expected to exhibit less oxide disruption, and hence less hydride formation sites, than the other samples since its surface exposed length of metal grain boundary was diminished (because grain size was substantially greater). This was exactly as we observed. In other relevant studies, thermal annealing has been observed to increase the bulk hydriding rate of uranium [36] and the growth rate of individual hydrides growth sites [19] as well as promoting steady state reaction kinetics [25]. However, to achieve a fully-formed reaction front, and reach the bulk reaction stage, the existing hydrides should grow sufficiently to coalesce. Internal stresses and grain boundaries of certain orientations may hinder hydride development by limiting UH_3 growth at their interface [41]. Thus, for certain geometries and environmental conditions, this could potentially lead to a non-uniform attack of the metal [18].

It should be noted that our experimental set-up was not designed to investigate whether the subsequent growth kinetics of individual nucleation sites was comparably higher on the annealed sample than for the others due to modification of the microstructure and removal of strain [19]. However, the observation of 'large family' hydrides only on the work-hardened sample, is potentially suggestive that either (1) hydride nucleation occurred earlier or (2) the growth velocity was more rapid for this population. If the latter is correct then it is suggested that this promoted by the enhanced level of strain in the work-hardened

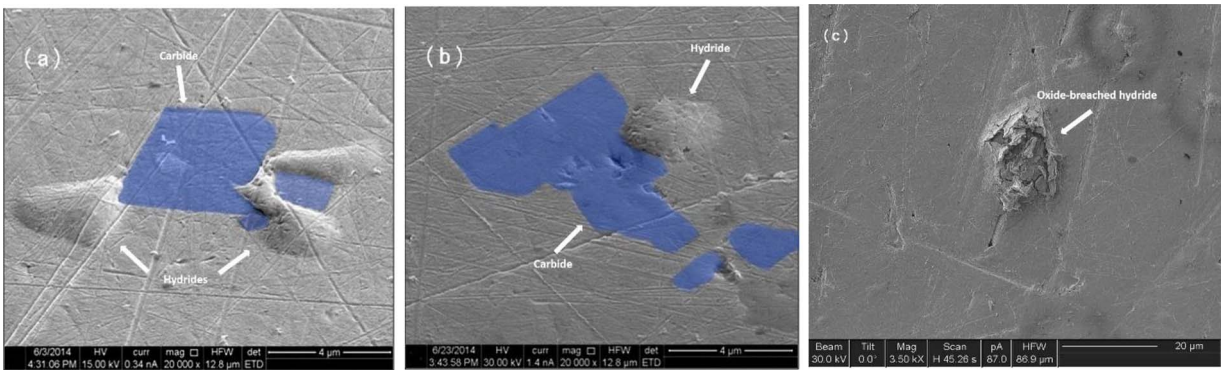

Fig. 7. Secondary electron (SE) images of (a) hydrides forming on the periphery of a carbide inclusion on the as-cast uranium surface; (b) a hydride forming at the margins of a carbide on the thermally annealed sample surface and (c) a hydride breaching the oxide locally, and nucleating at a carbide inclusion on the work-hardened sample. Carbides are highlighted in light-blue.

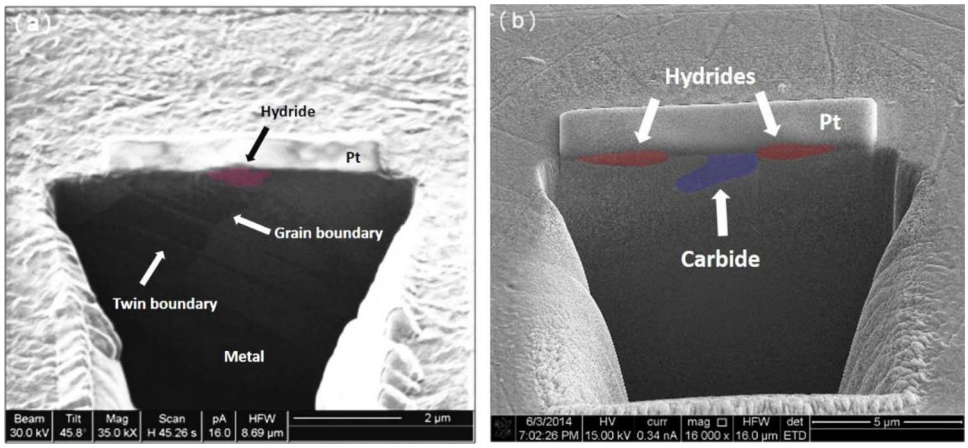

Fig. 8. Secondary electron (SE) images of focused ion beam cross-sectional cuts into the as-cast uranium sample showing (a) a hydride forming around a grain boundary site and (b) two hydrides forming around the margins of a carbide inclusion. Platinum (Pt) was deposited over the exposed UH3 surface to minimise disruption of the hydride during the etching process.

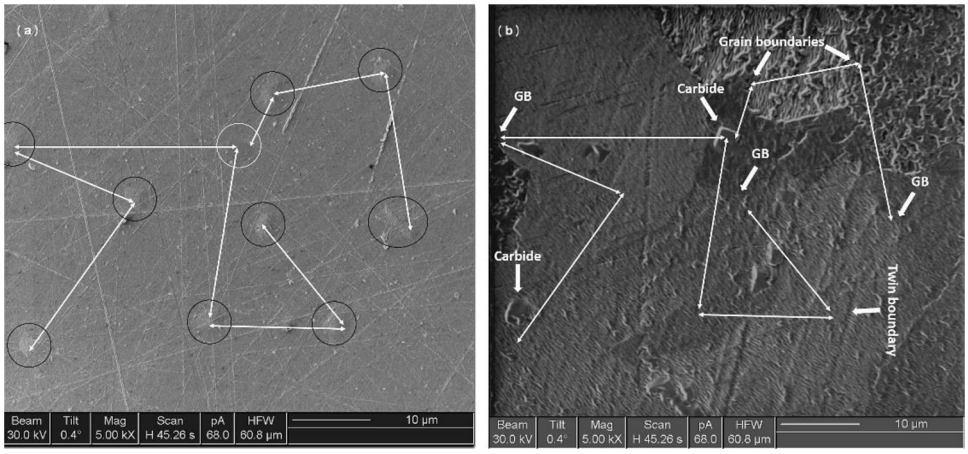

Fig. 9. Secondary electron (SE) image showing the surface of the thermally annealed sample (a) prior to and (b) following ion-sputtering (at 6600 pA probe current, 0.035 mm2, 90° angle of incidence for 5 min). The carbide and the hydride locations are circled in white and black, respectively. Equidistant arrows between relative locations of UH3 and carbide sites were used on (a) and (b) in order for the specific location of the UH3 growths to be identified on (b).

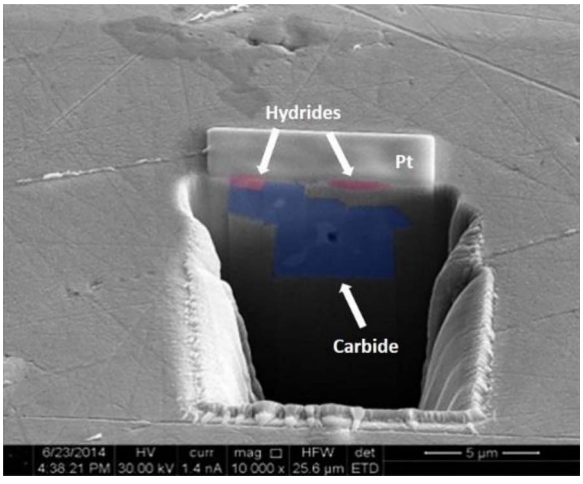

Fig. 10. Secondary electron (SE) image of a cross-section into the thermally annealed sample showing two hydrides forming on the margins of cuboid-shaped carbide inclusion. Platinum (Pt) was deposited over the exposed UH3 surface to minimise disruption of the hydride during the etching process.

layer of the reacting metal. Certainly, this matches with the findings of a recent study by Banos et al. [30], which indicated that the hydride propagation rate in the metal was enhanced in a work-hardened region in comparison to a strain-free region.

Interestingly, the work-hardened sample exhibited the lowest nucleation number density of hydride growth sites of all three samples, despite exhibiting the greatest surface strain, greatest metal grain boundary length and the greatest mass of formed hydride (determined by simple geometrical calculations assuming elliptical hydride morphology – not shown here). Jones et al. [37] observed the same behaviour and attributed the effect to the unevenness of the growing oxide on the damaged surface. Our earlier work with respect to the effect of differential surface preparation on early hydriding suggested that the existing work-hardened layer on the mechanically abraded samples resulted in high nucleation rate and an almost fully formed reaction front (a near continuous but thin hydride layer) with most of the UH_3 not breaching the oxide [30]. On the deliberately work-hardened surface produced for this work, contrary to previous observations [30], the nucleation rate was rather moderate but a significant population of larger oxide-breaching hydride growth sites was observed. This different behaviour is believed to occur due to the considerably higher level of deformation in the metal at the surface of the work-hardened sample, providing sites which offer either faster hydrogen ingress, earlier nucleation (than elsewhere) and/or enhanced growth kinetics. Once the oxide is breached by a population of growth sites, any further hydride formation is expected to occur as growth exclusively around those breached hydride growths, starving the other smaller sites of hydrogen and limiting any further nucleation elsewhere on the surface [42].

To summarise, from the analysis it was found that the volume of uranium hydride formation was greatest on the sample exhibiting the greatest degree of strain and grain boundary length, despite it exhibiting the lowest number density of nucleation sites. Only the work-hardened uranium surface exhibited two hydride growth families (Fig. 12): (1) a small diameter nucleating group associated mostly with grain/twin boundaries and surface strained regions; and (2) a group of large oxide-ruptured nucleation sites, observed to form around carbides, oxide discontinuities and highly strained striation zones. Carbide

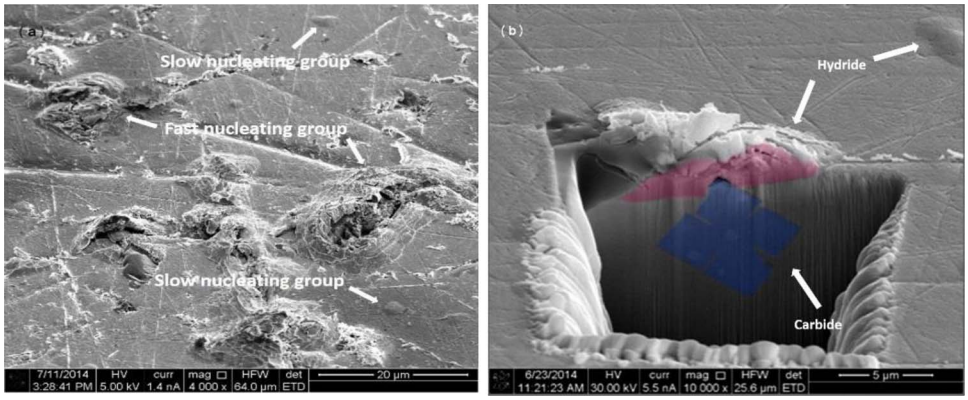

Fig. 11. Secondary electron (SE) images of the work-hardened sample showing (a) two hydride family types (small diameter and large diameter) observed to nucleate at the surface, and (b) focused ion beam (FIB) cross-sectional image of a large diameter hydride forming at an X-type carbide inclusion.

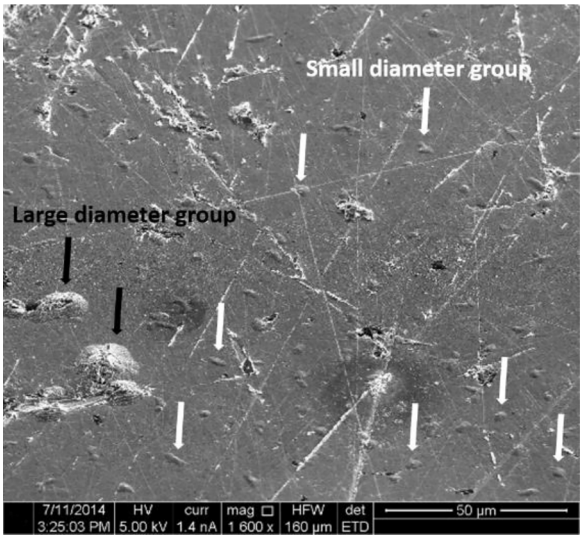

Fig. 12. Secondary electron (SE) image of the work-hardened surface highlighting the abundance of the small diameter group on certain areas of the sample surface.

inclusions also played a key role in the nucleation of hydride growths on all three surfaces, with almost two-thirds of the observed carbides acting as nuclei for hydride growth.

Thermally treating the sample caused the hydride nucleation number density to diminish relative to the as-received sample, however, the hydriding characteristics remained very similar.

5. Conclusions

The work presented here highlights the distinct differences in the rate and morphology of hydrogen-induced corrosion occurring due to differences in the level of induced stress/strain at the surface of uranium metal. By following almost identical finishing preparation of the surfaces and reacting all three samples in the same cell, providing identical sample degassing and hydride formation conditions, it has been confirmed that:

i. The mass of hydride as well as surface damage, caused per hydride, decreased as we move from a work-hardened to an as-cast and then a thermally annealed metal surface.
ii. Carbide inclusions played a key role in controlling the location of hydride nucleation on all three surfaces, with almost two-thirds of the observed carbide sites acting as nuclei for hydride growth.
iii. Vacuum annealing of uranium at a high temperature (550 °C) and for prolonged period (140 h) (prior to surface preparation) produced a relatively stress-free sample where recrystallisation, grain growth and twin boundary reduction was observed.
iv. By reducing the grain/twin boundary length, the number of hydride nucleation points per unit area was found to decrease. The comparison was made to the as-cast sample which exhibited similar hydriding behaviour.
v. Cold work-hardening of the metal surface, imparted strain which most quantifiably manifest as an increase in the number of twin boundaries. This had the effect of significantly altering the corrosion behaviour of the metal surface.

Acknowledgements

The authors would like to thank the Engineering and Physical Sciences Research Council (EPSRC) and Sellafield Ltd for funding this project as part of 42-month PhD research studentship (Ref: 1338575) at the Interface Analysis Centre (IAC), School of Physics, University of Bristol. Also, would like to thank Mr John Jowsey and Dr Anna Adamska from the Sellafield Centre of Expertise in Uranium and Reactive Metals (URM) for contextual guidance and technical input.

References

[1] T. Totemeier, R. Pahl, S. Hayes, S. Frank, Characterization of corroded metallic uranium fuel plates, J. Nucl. Mater. 256 (1998) 87–95.
[2] R. Orr, H. Godfrey, C. Broan, D. Goddard, G. Woodhouse, P. Durham, A. Diggle, J. Bradshaw, Formation and physical properties of uranium hydride under conditions relevant to metallic fuel and nuclear waste storage, J. Nucl. Mater. 477 (2016) 236–245.
[3] C. Stitt, N. Harker, K. Hallam, C. Paraskevoulakos, A. Banos, S. Rennie, J. Jowsey, T. Scott, An investigation on the persistence of uranium hydride during storage of simulant nuclear waste packages, PLoS One 10 (2015) e0132284.
[4] F. Le Guyadec, X. Génin, J. Bayle, O. Dugne, A. Duhart-Barone, C. Ablitzer, Pyrophoric behaviour of uranium hydride and uranium powders, J. Nucl. Mater. 396 (2010) 294–302.
[5] C. Ablitzer, F. Le Guyadec, J. Raynal, X. Génin, A. Duhart-Barone, Influence of superficial oxidation on the pyrophoric behaviour of uranium hydride and uranium powders in air, J. Nucl. Mater. 432 (2013) 135–145.
[6] R. Alire, B. Mueller, C.L. Peterson, J.R. Mosley, Reaction kinetics of uranium and deuterium, J. Chem. Phys. 52 (1970) 37–46.
[7] J. Condon, E. Larson, Kinetics of the uranium-hydrogen system, J. Chem. Phys. 59 (1973) 855–865.
[8] J. Condon, Alternative model for nonstoichiometry in uranium hydride, J. Phys. Chem. 79 (1975) 42–48.
[9] J. Condon, vs. Calculated, experimental hydrogen reactions rates with uranium, J. Phys. Chem. 79 (1975) 392–397.
[10] J. Stakebake, Kinetics for the reaction of hydrogen with uranium powder, J. Electrochem. Soc. 126 (1979) 1596–1601.
[11] J. Bloch, M. Mintz, Kinetics and mechanism of the UH reaction, J. Less Common Met. 81 (1981) 301–320.
[12] J. Kirkpatrick, J. Condon, The linear solution for hydriding of uranium, J. Less Common Met. 172 (1991) 124–135.
[13] G. Powell, W. Harper, J. Kirkpatrick, The kinetics of the hydriding of uranium metal, J. Less Common Met. 172 (1991) 116–123.
[14] G. Powell, R. Ceo, W. Harper, J. Kirkpatrick, The kinetics of the hydriding of uranium metal II*, Zeitschrift für Physikalische Chemie 181 (1993) 275–282.
[15] S. Bazley, T. Nunney, C. Mormiche, B. Hayden, The dynamics of hydrogen adsorption on polycrystalline uranium, Appl. Surf. Sci. 254 (2008) 6376–6379.
[16] R. Arkush, A. Venkert, M. Aizenshtein, S. Zalkind, D. Moreno, M. Brill, M. Mintz, N. Shamir, Site-related nucleation and growth of hydrides on uranium surfaces, J.

Alloys Compd. 244 (1996) 197–205.
[17] J. Bloch, F. Simca, M. Kroup, A. Stern, D. Shmariahu, M. Mintz, Z. Hadari, The initial kinetics of uranium hydride formation studied by a hot-stage microscope technique, J. Less Common Met. 103 (1984) 163–171.
[18] J. Bloch, D. Brami, A. Kremner, M. Mintz, Effects of gas phase impurities on the topochemical-kinetic behaviour of uranium hydride development, J. Less Common Met. 139 (1988) 371–383.
[19] J. Bloch, M.H. Mintz, The effect of thermal annealing on the hydriding kinetics of uranium, J. Less Common Met. 166 (1990) 241–251.
[20] D. Moreno, R. Arkush, S. Zalkind, N. Shamir, Physical discontinuities in the surface microstructure of uranium alloys as preferred sites for hydrogen attack, J. Nucl. Mater. 230 (1996) 181–186.
[21] D.F. Teter, R.J. Hanrahan, C.J. Wetteland, Uranium Hydride Nucleation Kinetics: Effects of Oxide Thickness and Vacuum Outgassing, Los Alamos National Lab., NM (US), 2001.
[22] T.B. Scott, G.C. Allen, I. Findlay, J. Glascott, UD_3 formation on uranium: evidence for grain boundary precipitation, Philos. Mag. 87 (2007) 177–187.
[23] J. Knowles, I. Findlay, D. Geeson, S. Bazley, The influence of vacuum annealing on the nucleation and growth kinetics of uranium hydride, MRS Proceedings, Cambridge Univ Press, 2012 pp. mrss12-1444-y1410-1410.
[24] N. Harker, T. Scott, C. Jones, J. Petherbridge, J. Glascott, Altering the hydriding behaviour of uranium metal by induced oxide penetration around carbo-nitride inclusions, Solid State Ionics 241 (2013) 46–52.
[25] J.P. Knowles, I.M. Findlay, The influence of vacuum annealing on the uranium-hydrogen reaction, J. Alloys Compd. 645 (2015) S230–S233.
[26] P. Shi, F. Li, Y. Wu, H. Ji, R. Li, X. Wang, Effect of alloyed Ti on the microstructure and corrosion characteristics of a U–Ti alloy in a hydrogen environment, Corros. Sci. 93 (2015) 58–62.
[27] J. Bloch, M.H. Mintz, Kinetics and mechanisms of metal hydrides formation—a review, J. Alloys Compd. 253 (1997) 529–541.
[28] C. Stitt, M. Hart, N. Harker, K. Hallam, J. MacFarlane, A. Banos, C. Paraskevoulakos, E. Butcher, C. Padovani, T. Scott, Nuclear waste viewed in a new light; a synchrotron study of uranium encapsulated in grout, J. Hazard. Mater. 285 (2015) 221–227.
[29] C. Stitt, C. Paraskevoulakos, N. Harker, A. Banos, K. Hallam, C. Jones, T. Scott, Real-time, in-situ deuteriding of uranium encapsulated in grout; effects of temperature on the uranium-deuterium reaction, Corros. Sci. 127 (2017) 270–279.
[30] A. Banos, C. Stitt, T. Scott, The effect of sample preparation on uranium hydriding, Corros. Sci. 113 (2016) 91–103.
[31] C. Stitt, C. Paraskevoulakos, N. Harker, C. Jones, T. Scott, The effects of metal surface geometry on the formation of uranium hydride, Corros. Sci. 98 (2015) 63–71.
[32] A. Banos, T.B. Scott, Statistical analysis of UH_3 initiation using electron back-scattered diffraction (EBSD), Solid State Ionics 296 (2016) 137–145.
[33] A. Ennos, The origin of specimen contamination in the electron microscope, Br. J. Appl. Phys. 4 (1953) 101.
[34] A. Ennos, The sources of electron-induced contamination in kinetic vacuum systems, Br. J. Appl. Phys. 5 (1954) 27.
[35] A. Griffiths, T. Walther, Quantification of carbon contamination under electron beam irradiation in a scanning transmission electron microscope and its suppression by plasma cleaning, J. Phys. Conf. Ser. IOP Publ. (2010) 12–17.
[36] A. DeMint, J. Leckey, Effect of silicon impurities and heat treatment on uranium hydriding rates, J. Nucl. Mater. 281 (2000) 208–212.
[37] C.P. Jones, T.B. Scott, J.R. Petherbridge, J. Glascott, A surface science study of the initial stages of hydrogen corrosion on uranium metal and the role played by grain microstructure, Solid State Ionics 231 (2013) 81–86.
[38] A. Danon, J. Koresh, M. Mintz, Temperature-programmed desorption characterization of oxidized uranium surfaces: relation to some gas-uranium reactions, Langmuir 15 (1999) 5913–5920.
[39] P. Weber, J. Matzel, I. Hutcheon, Analyses of U Metal for H, C and O, Lawrence Livermore National Laboratory (LLNL), Livermore, CA, 2012.
[40] J. Petherbridge, J. Knowles, S. Bazley, The effect of thermal pre-treatments on the nucleation of uranium hydride, Solid State Ionics 292 (2016) 110–115.
[41] M.P. Adamson, S. Orman, G. Picton, The effects of hydrogen on the tensile properties of uranium when tested in different environments, J. Nucl. Mater. 33 (1969) 215–224.
[42] C.P. Jones, T.B. Scott, J.R. Petherbridge, Structural deformation of metallic uranium surrounding hydride growth sites, Corros. Sci. 96 (2015) 144–151.